LETTER

https://doi.org/10.1038/s41586-018-0592-2

Electronic noise due to temperature differences in atomic-scale junctions

Ofir Shein Lumbroso[1], Lena Simine[2,3], Abraham Nitzan[4,5], Dvira Segal[2] & Oren Tal[1]*

Since the discovery a century ago[1–3] of electronic thermal noise and shot noise, these forms of fundamental noise have had an enormous impact on science and technology research and applications. They can be used to probe quantum effects and thermodynamic quantities[4–11], but they are also regarded as undesirable in electronic devices because they obscure the target signal. Electronic thermal noise is generated at equilibrium at finite (non-zero) temperature, whereas electronic shot noise is a non-equilibrium current noise that is generated by partial transmission and reflection (partition) of the incoming electrons[8]. Until now, shot noise has been stimulated by a voltage, either applied directly[8] or activated by radiation[12,13]. Here we report measurements of a fundamental electronic noise that is generated by temperature differences across nanoscale conductors, which we term 'delta-T noise'. We experimentally demonstrate this noise in atomic and molecular junctions, and analyse it theoretically using the Landauer formalism[8,14]. Our findings show that delta-T noise is distinct from thermal noise and voltage-activated shot noise[8]. Like thermal noise, it has a purely thermal origin, but delta-T noise is generated only out of equilibrium. Delta-T noise and standard shot noise have the same partition origin, but are activated by different stimuli. We infer that delta-T noise in combination with thermal noise can be used to detect temperature differences across nanoscale conductors without the need to fabricate sophisticated local probes. Thus it can greatly facilitate the study of heat transport at the nanoscale. In the context of modern electronics, temperature differences are often generated unintentionally across electronic components. Taking into account the contribution of delta-T noise in these cases is likely to be essential for the design of efficient nanoscale electronics at the quantum limit.

At non-zero temperature, the thermal motion of electrons leads to temporal current fluctuations referred to as the thermal (Johnson–Nyquist) noise S_{TN}, even at zero net current, in equilibrium conditions[2,3]. This noise depends on the conductance G ($G=1/R$, where R is the resistance) and temperature T in a straightforward manner[8], $S_{TN}=4k_BTG$, where k_B is Boltzmann's constant. Thermal noise can be used as a primary thermometer, and it does not depend on the conductor's shape, material type or the details of the transport mechanism[4,15]. When current is generated across a conductor, electrons can either be transmitted through the conductor or backscatter, leading to non-equilibrium temporal current fluctuations called electronic shot noise. This noise has been extensively used in the study of electronic transport in quantum conductors, including the analysis of quasiparticles' charge, electronic spin transport, and interacting many-body systems[5,6,9,10]. Shot noise measurements also provide unique information about electronic transport at the miniaturization limit of electronic conductors, namely across atomic and molecular junctions[7,16–21]. These junctions are composed of individual atoms or molecules suspended between two electrodes. The conductance of such quantum coherent conductors is described by the Landauer formalism as the sum of contributions from several transmission channels[8], $G=G_0\sum_i \tau_i$. Here τ_i is the transmission probability of the ith channel, and it can take any value between zero (closed channel) to one (fully open channel). G_0 is the quantum of conductance; $G_0 \approx (12.9\ \mathrm{k\Omega})^{-1}$. In the Landauer framework, the current noise in spin-degenerate quantum conductors, including both thermal and shot noises, can be described as[7,8]

$$S_I = 4k_BTG_0\sum_i \tau_i^2 + 2eV\coth\left(\frac{eV}{2k_BT}\right)G_0\sum_i \tau_i(1-\tau_i) \qquad (1)$$

where e and V are the electron charge and the applied voltage across the conductor, respectively. At zero applied voltage, the contribution of shot noise is nullified (that is, for $eV \ll k_BT$ the second term collapses to $4k_BTG_0\sum_i \tau_i(1-\tau_i)$) and equation (1) reduces to the thermal noise.

When a temperature difference ΔT, instead of a voltage difference, is applied across the conductor, a new approximate expression for the current noise can be derived based on the Landauer formalism:

$$S_I \approx 4k_B\bar{T}G_0\sum_i \tau_i + \left[\frac{k_B(\Delta T)^2}{\bar{T}}\left(\frac{\pi^2}{9}-\frac{2}{3}\right)\right]G_0\sum_i \tau_i(1-\tau_i) \qquad (2)$$

Here, $\bar{T}$ is the arithmetic average of T_h and T_c, the temperatures at the hot and cold sides of the conductor (Fig. 1a), and $\Delta T = T_h - T_c$. An expression for the noise generated by temperature difference has been previously derived for diffusive conductors[22]. The full derivation of equation (2), including additional terms and more general expressions, appears in Supplementary Information. The first term corresponds to the thermal noise. However, when a temperature difference is applied, this term depends on the average temperature across the conductor. Remarkably, a new noise contribution (the second term), which we denote as delta-T noise, is generated as a result of the temperature difference across the conductor. In contrast to standard voltage-activated shot noise, delta-T noise has a pure thermal origin. Yet, similarly to standard shot noise, it depends on the factor $\sum_i \tau_i(1-\tau_i)$ despite the absence of a voltage gradient across the conductor. This dependence is a signature of electronic partition noise[8], namely, noise that is activated by the partial transmission and backscattering of transporting electrons. For delta-T noise, non-equilibrium conditions are introduced by a temperature difference and the partition noise is activated even in the ideal case of zero net charge current owing to opposite and equal currents above and below the chemical potential (Fig. 1b). Thus, delta-T noise can be viewed as shot noise that is generated by temperature difference.

To experimentally demonstrate the effect of temperature difference on the noise generated in a quantum conductor, we study molecular junctions based on hydrogen molecules introduced between two atomically sharp gold electrodes[23,24]. We use the break junction technique[25] (Fig. 1a and Methods) to form an ensemble of molecular junctions with different local structure and hence different conductance values (Extended Data Fig. 1). In contrast to bare gold atomic junctions, the hydrogen-based molecular junctions provide a wide span of conductance values below $1G_0$. Shot noise measurements indicate that below $1G_0$ the conductance of the formed molecular junctions is typically

[1]Department of Chemical and Biological Physics, Weizmann Institute of Science, Rehovot, Israel. [2]Department of Chemistry, University of Toronto, Toronto, Ontario, Canada. [3]Department of Chemistry, Rice University, Houston, TX, USA. [4]Department of Chemistry, University of Pennsylvania, Philadelphia, PA, USA. [5]School of Chemistry, Tel Aviv University, Tel Aviv, Israel. *e-mail: oren.tal@weizmann.ac.il

© 2018 Springer Nature Limited. All rights reserved.

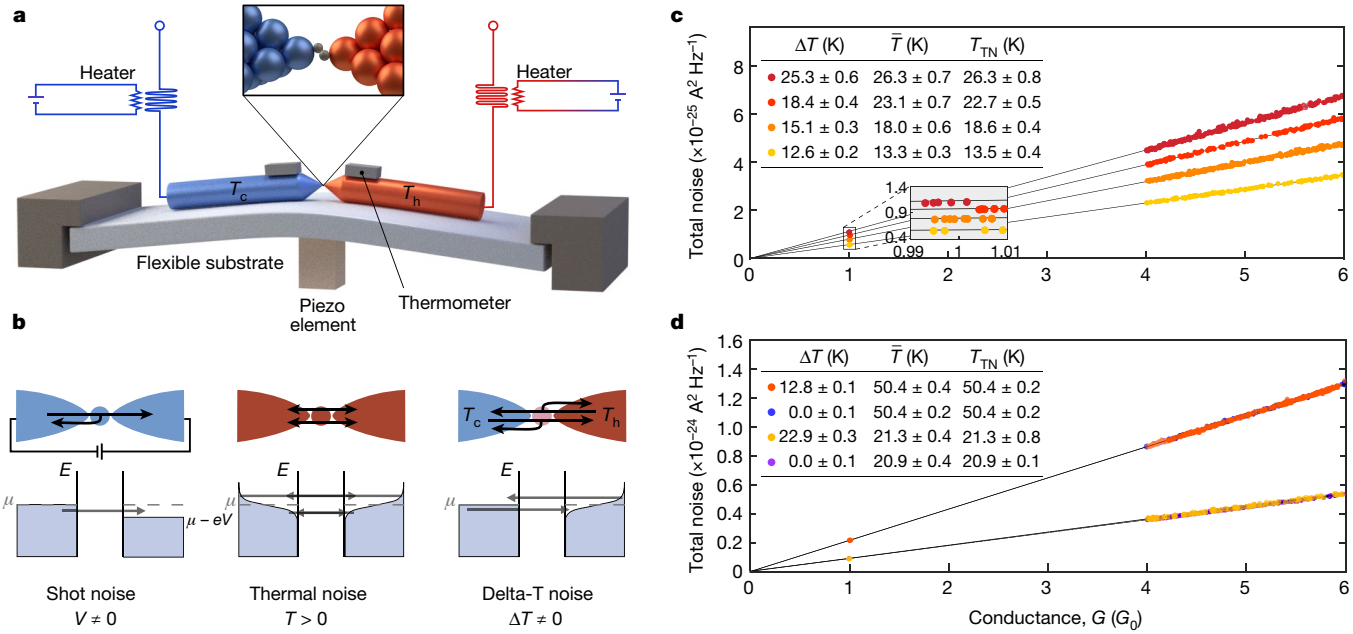

Fig. 1 | Experimental setup, noise contributions and measured total noise at a finite temperature difference. a, Schematic of the break junction setup, and the Au/H_2 junction. **b**, Illustration of the standard shot noise, thermal noise and delta-T noise generated in atomic-scale junctions. For simplicity, in the left and right schematics we assume $T=0$ and $T_c=0$, respectively. μ is the chemical potential; V is the applied voltage across the junction; e is the electron charge. **c**, Total noise as a function of conductance measured in Au/H_2 junctions at different temperatures T_h and T_c at the opposite sides of the junctions. The linear dependence of the noise on the conductance is expected when the total noise is dominated by the first term in equation (2) (thermal noise), while the second term (delta-T noise) is suppressed. This situation is expected at $1G_0$ and $>4G_0$. The inset tables present the temperature difference ΔT and average temperature $\bar{T}$ determined by the thermometers at the opposite sides of the junctions, and the thermal noise temperature T_{TN}, which is extracted from the slope of the total noise. For a given conductance, the thermal noise is exclusively determined by the average temperature of the hot and cold electrodes. **d**, Four sets of total noise data as in **c**. Each pair of datasets is taken at a similar $\bar{T}$, but one set is measured at $\Delta T \neq 0$ and the other at $\Delta T=0$. The data presented illustrate that a comparable thermal noise is generated at different ΔT values, as long as $\bar{T}$ is identical. The error bars of the total noise data, corresponding to the systematic errors in our measurements, are smaller than the diameter of the symbols. Nine measurement sets at different ΔT were collected on three different samples with similar results. In each presented set, 91–301 junctions were realized and measured.

governed by a single dominant transmission channel, with minor contributions from secondary channels (see Methods and Extended Data Fig. 4). The transmission probabilities of these channels can be varied, for example, by adjusting the separation between the electrodes in sub-ångström resolution[25]. A temperature gradient across the junction was applied by an asymmetric heating of the junction's electrodes above a base 4.2 K. The temperature difference across the junction was monitored by two thermometers located at opposite sides of the junction (Fig. 1a). To determine the temperature at the nanoscale vicinity of the junction, the thermometers were calibrated using the thermal noise generated in the junction, when no temperature difference was applied (see Methods).

Equation (2) represents current noise due to temperature difference across a quantum coherent conductor as an additive combination of a standard thermal noise, yet proportional to the average temperature, and a new contribution associated with thermal difference. To test the validity of the first term in equation (2), we consider cases where a temperature gradient is applied across the examined junctions, while the second term (delta-T noise) is suppressed. Practically, this situation can be met in two ways. When the conductance of the studied junction is dominated by a single channel with transmission probability close to one ($\tau \approx 1$), the second term is expected to be very small. This condition is indeed achieved in some junction realizations, as indicated by shot noise measurements (Extended Data Fig. 4). Furthermore, the relative contribution of the second term with respect to the first one depends on $(\Delta T/\bar{T})^2$ and the Fano factor $F=\sum_i \tau_i(1-\tau_i)/\sum_i \tau_i$. The Fano factor can be determined by shot noise measurements on similar junctions. We found that if the junction is squeezed to form a multi-atomic gold contact[7] with a conductance above $4G_0$, the maximal contribution of the second term in equation (2) is less than 5% of the magnitude of the first term in the examined conditions, and typically around 3% (see Methods and Extended Data Fig. 4).

In Fig. 1c we show the measured total noise as a function of conductance (see Methods) for the studied junctions at different average junction temperature and temperature difference, determined by the calibrated thermometers at the hot and cold sides of the junction. We attribute the linear dependence of the noise on the conductance to efficient suppression of the second term in equation (2) at $1G_0$ and above $4G_0$. In these conditions, the total noise is practically reduced to the thermal noise, and the temperature associated with the thermal noise T_{TN} can be extracted from the slope of each curve. The inset table in Fig. 1c shows that $T_{TN}=\bar{T}$ within the error range, indicating that the thermal noise generated in the junction depends on the average temperature of the junction. Figure 1d presents two examples for total noise versus conductance measured at comparable average temperature of about $\bar{T}=21$ K, as well as $\bar{T}=50$ K. In each example, the temperature difference across the examined junction is set to be either zero ($\Delta T=0$) or finite ($\Delta T \neq 0$), as seen in the inset table. The data points clearly fall on top of each other, illustrating that the thermal noise is exclusively determined by the average temperature and that it is independent on the temperature difference.

We now focus on the identification of the delta-T noise, and its properties. Figure 2 presents measurements of excess noise as a function of conductance for different temperature differences and average temperatures. We examined the conductance range $0.1 < G < 1G_0$ to look for a possible $\tau(1-\tau)$ dependence of the delta-T noise. The excess noise is defined as the total noise minus the average thermal noise. The latter is obtained as presented in Fig. 1c and explained above. The sets of measurements at $\Delta T=0$ K (Fig. 2a–c) show data around zero excess noise. In the absence of temperature difference, the total noise is governed by the thermal noise. Therefore, subtracting the average thermal

© 2018 Springer Nature Limited. All rights reserved.

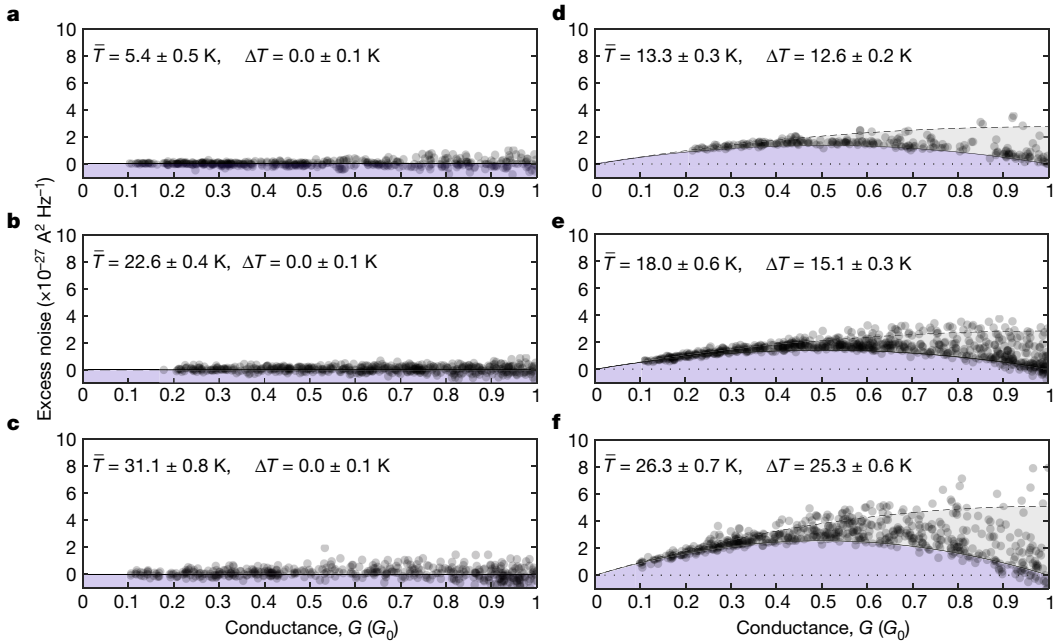

Fig. 2 | Excess noise measured at zero and finite temperature difference. **a**–**c**, Excess noise (obtained by subtracting the average thermal noise from the total measured noise) versus conductance measured in the molecular junctions examined at different temperatures at thermal equilibrium ($\Delta T = 0$). **d**–**f**, Excess noise versus conductance measured at different average temperatures and finite temperature differences across the junctions ($\Delta T \neq 0$). Calculated delta-T noise is given by the black curve for a single transmission channel, and by the dashed curve for two channels with equal transmission probabilities (non-approximated numerical calculations based on equation (S2) in Supplementary Information). The error bars, corresponding to the systematic errors in our measurements, are comparable or slightly larger than the diameter of the dark semitransparent symbols, as shown in Extended Data Fig. 7. When a temperature difference is applied across the junctions, a clear enhancement of the excess noise is observed. The measured excess noise can be described by the theoretical expression for the delta-T noise. The spread in the results is a natural outcome of additional transmission channels that open up as the conductance increases (see Extended Data Fig. 4). Eight measurement sets at different ΔT were collected on three different samples with similar results. In each presented set, 248–716 junctions were realized and measured.

noise from the total noise gives values that are scattered around zero. Remarkably, when a temperature difference is applied across the junction, an excess noise is activated (Fig. 2d–f), indicating that the origin of the measured noise is temperature difference. We note that even in the absence of applied voltage, the thermoelectric effect can generate voltage in the presence of a temperature difference[26]. This thermoelectric voltage produces shot noise that can be detected as an excess noise at a finite temperature difference. However, in the examined junctions, when no external voltage is applied, the expected shot noise due to the thermoelectric voltage is about three orders of magnitude lower than the measured excess noise in Fig. 2d–f. This is illustrated in Extended Data Fig. 6, by measuring the total thermoelectric voltage produced in our experiments and calculating the shot noise that can be generated by the highest thermoelectric voltage that was found (see Methods). We therefore conclude that the contribution of shot noise due to the generated thermoelectric voltage (in the absence of applied voltage) is negligible with respect to the measured excess noise at a finite temperature difference, and cannot explain its origin.

In Fig. 2d–f, the dependence of the low-lying noise data on the conductance is well described by the solid curve, which provides the calculated delta-T noise, assuming a single transmission channel. In fact, the majority of the data points accumulate in the vicinity of this curve, indicating the activation of delta-T noise in junctions with a dominant conductance contribution from a single transmission channel. As the conductance increases, the spread of the measured noise towards higher values increases as well. This characteristic trend is captured by the dashed line that gives the calculated delta-T noise for junctions with two channels of equal transmission probabilities ($\tau_1 = \tau_2$ and $\tau_1 + \tau_2 = G/G_0$). Shot noise measurements and numerical channel analysis (see Methods and Extended Data Fig. 4) indicate that most of the examined molecular junctions are characterized by transport via a dominant channel, yet some junctions can have a large and even comparable conductance contribution from a second channel. Additional channels, beyond the first two, usually have either a minor contribution or no contribution. From this channel analysis, delta-T noise is expected to yield excess noise data that are mainly located within the grey region, as we indeed observe. Thus, the characteristics of the measured excess noise fit the expected behaviour of delta-T noise in the examined junctions. Similar measurements were performed on bare gold atomic junctions, yet with a very limited span of conductance below $1G_0$ (Extended Data Fig. 8). Using equation (2), we can extract the Fano factor from the excess noise that is generated by temperature difference. Extended Data Fig. 9 shows that the Fano factor distribution acquired in this way and plotted versus conductance is similar to the one obtained by voltage-activated shot noise measurements (Extended Data Fig. 4). This comparison further demonstrates that the excess noise at finite temperature difference is the delta-T noise described by the second term of equation (2).

The quadratic dependence of the delta-T noise on temperature difference is a distinctive fingerprint of this noise. To check whether the detected excess noise shows the expected dependence on temperature difference, we normalize the measured excess noise, based on equation (2), and plot it with respect to ΔT in Fig. 3. The normalization is given in the caption of Fig. 3, assuming a single channel. The data spread for each ΔT is asymmetric and can be described by a generalized extreme value distribution (inset to Fig. 3). The red rectangles in Fig. 3 give the most probable values of the normalized excess noise, which are determined by the peak of the fit to the data distribution (see the inset of Fig. 3) for each temperature difference. The dashed curve in the main panel of Fig. 3 depicts the quadratic dependence of the delta-T noise on the temperature difference for a single channel scenario, and it fits very well the most probable normalized excess noise. The upward spread of the data (transparent circles) is attributed to the presence of junctions with more than one transmission channel, since the noise at

© 2018 Springer Nature Limited. All rights reserved.

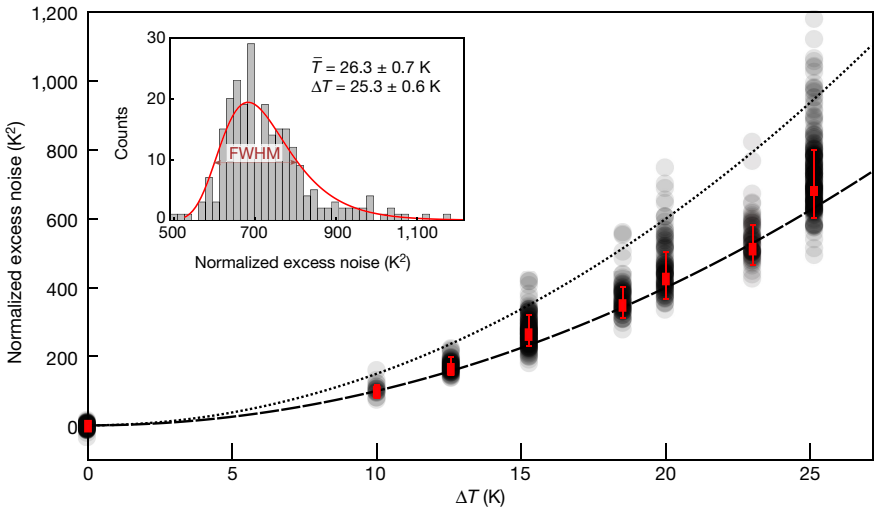

Fig. 3 | Excess noise dependence on the applied temperature difference. Normalized excess noise as a function of ΔT (black semitransparent symbols). To test the possible $(\Delta T)^2$ dependence expected for the delta-T noise, the measured excess noise between $0.1G_0$ and $0.5G_0$ was normalized (by dividing by $k_B G_0 \tau(1-\tau)(\pi^2/9-2/3)/T_{TN}$ on the basis of the second term in equation (2)), assuming $\bar{T} = T_{TN}$. The dashed line shows the calculated normalized delta-T noise for the case of a single transmission channel, and the dotted line illustrates the calculated normalized delta-T noise for the case of two channels with equal transmission probabilities. The most probable normalized excess noise (red rectangles) shows a clear $(\Delta T)^2$ dependence, as expected for delta-T noise that is generated by a single channel. The inset shows the distribution of the normalized excess noise for $\Delta T = 25.3 \pm 0.6$ K. The most probable normalized excess noise is determined by the maximum of a fitted generalized extreme value distribution that captures the asymmetric distribution of the data. Error bars are determined by the full-width at half-maximum (FWHM) as illustrated in the inset. The measured excess noise is normalized assuming a single channel. As a result, the spread of the data (black transparent circles) is artificially increased towards higher values.

a given conductance is larger for a higher number of partially open channels, as a result of its dependence on $\sum_i \tau_i(1-\tau_i)$. Nevertheless, most of the data falls below the dotted curve, which shows the delta-T noise dependence on $(\Delta T)^2$ for the case of two channels with similar transmission probabilities. Observing this dependence provides a complementary indication that the measured noise behaves as expected for the delta-T noise.

To conclude, our experimental findings, supported by a theoretical derivation, demonstrate that electronic noise emerges in the presence of a temperature difference across quantum conductors. We term this noise contribution as the delta-T noise and show that it possesses a peculiar combination of characteristics that makes it distinct from the standard thermal noise and voltage-activated shot noise. Beyond the fundamental interest in the observation and characterization of a temperature-difference-based form of partition noise, the delta-T noise can be used (in combination with thermal noise) as a probe for temperature differences. This ability is particularly interesting for nanoscale systems since fabricating physical probes that measure local temperature at this scale is extremely challenging. In contrast to physical sensors, the delta-T noise is a versatile probe, which is not limited to a specific temperature range and can be applied to conductors of different sizes, down to the atomic scale. Delta-T noise measurements can be performed without particular design limitations and can be implemented in a variety of setups, including scanning probe microscopes, nanoscale devices and even in embedded systems, which are less accessible to temperature sensing. This flexibility makes the delta-T noise an attractive tool for the study of heat management, including thermoelectricity, heat pumping and heat dissipation, which are important processes in the context of energy saving and sustainable energy production. Finally, temperature gradients are often unintentionally produced in electronic circuits. Thus, in the process of electronics miniaturization towards the quantum limit, the delta-T noise could become a performance-limiting factor that should be suppressed by minimizing temperature gradients.

Online content

Any methods, additional references, Nature Research reporting summaries, source data, statements of data availability and associated accession codes are available at https://doi.org/10.1038/s41586-018-0592-2.

Received: 7 May 2018; Accepted: 20 August 2018;
Published online 10 October 2018.

1. Schottky, W. Über spontane Stromschwankungen in verschiedenen Elektrizitätsleitern. *Ann. Phys.* **362**, 541–567 (1918).
2. Johnson, J. B. Thermal agitation of electricity in conductors. *Nature* **119**, 50–51 (1927).
3. Nyquist, H. Thermal agitation of electric charge in conductors. *Phys. Rev.* **32**, 110–113 (1928).
4. White, D. R. et al. The status of Johnson noise thermometry. *Metrologia* **33**, 325–335 (1996).
5. Saminadayar, L., Glattli, D. C., Jin, Y. & Etienne, B. Observation of the e/3 fractionally charged Laughlin quasiparticle. *Phys. Rev. Lett.* **79**, 2526 (1997).
6. de Picciotto, R. et al. Direct observation of a fractional charge. *Nature* **389**, 162–164 (1997).
7. van den Brom, H. E. & van Ruitenbeek, J. M. Quantum suppression of shot noise in atom-size metallic contacts. *Phys. Rev. Lett.* **82**, 1526–1529 (1999).
8. Blanter, Y. M. & Büttiker, M. Shot noise in mesoscopic conductors. *Phys. Rep.* **336**, 1–66 (2000).
9. Roche, P. et al. Fano factor reduction on the 0.7 conductance structure of a ballistic one-dimensional wire. *Phys. Rev. Lett.* **93**, 116602 (2004).
10. Delattre, T. et al. Noisy Kondo impurities. *Nat. Phys.* **5**, 208–212 (2009).
11. Jezouin, S. et al. Controlling charge quantization with quantum fluctuations. *Nature* **536**, 58–62 (2016).
12. Schoelkopf, R. J., Kozhevnikov, A. A., Prober, D. E. & Rooks, M. J. Observation of 'photon-assisted' shot noise in a phase-coherent conductor. *Phys. Rev. Lett.* **80**, 2437 (1998).
13. Reydellet, L.-H., Roche, P., Glattli, D. C., Etienne, B. & Jin, Y. Quantum partition noise of photon-created electron-hole pairs. *Phys. Rev. Lett.* **90**, 176803 (2003).
14. Büttiker, M., Imry, Y., Landauer, R. & Pinhas, S. Generalized many-channel conductance formula with application to small rings. *Phys. Rev. B* **31**, 6207 (1985).
15. Giazotto, F., Heikkilä, T. T., Luukanen, A., Savin, A. M. & Pekola, J. P. Opportunities for mesoscopics in thermometry and refrigeration: physics and applications. *Rev. Mod. Phys.* **78**, 217 (2006).
16. Djukic, D. & van Ruitenbeek, J. M. Shot noise measurements on a single molecule. *Nano Lett.* **6**, 789–793 (2006).
17. Tal, O., Krieger, M., Leerink, B. & van Ruitenbeek, J. M. Electron-vibration interaction in single-molecule junctions: from contact to tunneling regimes. *Phys. Rev. Lett.* **100**, 196804 (2008).
18. Chen, R., Matt, M., Pauly, F., Cuevas, J. C. & Natelson, D. Shot noise variation within ensembles of gold atomic break junctions at room temperature. *J. Phys. Condens. Matter* **26**, 474204 (2014).
19. Burtzlaff, A., Weismann, A., Brandbyge, M. & Berndt, R. Shot noise as a probe of spin-polarized transport through single atoms. *Phys. Rev. Lett.* **114**, 016602 (2015).
20. Vardimon, R., Klionsky, M. & Tal, O. Indication of complete spin filtering in atomic-scale nickel oxide. *Nano Lett.* **15**, 3894–3898 (2015).

© 2018 Springer Nature Limited. All rights reserved.

21. Karimi, M. A. et al. Shot noise of 1, 4-benzenedithiol single-molecule junctions. *Nano Lett.* **16**, 1803–1807 (2016).
22. Sukhorukov, E. V. & Loss, D. Noise in multiterminal diffusive conductors: Universality, nonlocality, and exchange effects. *Phys. Rev. B* **59**, 13054 (1999).
23. Csonka, S., Halbritter, A. & Mihály, G. Pulling gold nanowires with a hydrogen clamp: strong interactions of hydrogen molecules with gold nanojunctions. *Phys. Rev. B* **73**, 075405 (2006).
24. Nakazumi, T., Kaneko, S. & Kiguchi, M. Electron transport properties of Au, Ag, and Cu atomic contacts in a hydrogen environment. *J. Phys. Chem. C* **118**, 7489–7493 (2014).
25. Muller, C. J., van Ruitenbeek, J. M. & De Jongh, L. J. Experimental observation of the transition from weak link to tunnel junction. *Physica C* **191**, 485–504 (1992).
26. Reddy, P., Jang, S. Y., Segalman, R. A. & Majumdar, A. Thermoelectricity in molecular junctions. *Science* **315**, 1568–1571 (2007).

Acknowledgements O.T. appreciates the support of the Harold Perlman family, and acknowledges funding by a research grant from Dana and Yossie Hollander, the Israel Science Foundation (grant number 1089/15), and the Minerva Foundation (grant number 120865). D.S. acknowledges support from an NSERC Discovery Grant and the Canada Research Chair programme. The research of A.N. is supported by the US National Science Foundation (grant number CHE1665291), the Israel-US Binational Science Foundation, the German Research Foundation (DFG TH 820/11-1) and the University of Pennsylvania. L.S. acknowledges the Special Opportunity Graduate Travel Fellowship from the Department of Chemistry, University of Toronto.

Reviewer information *Nature* thanks E. Scheer and the other anonymous reviewer(s) for their contribution to the peer review of this work.

Author contributions The project was conceived by O.T. The experiments were designed by O.S.L. and O.T., and performed by O.S.L., under the supervision of O.T. The theoretical derivation was performed by L.S., A.N. and D.S. The manuscript was written by O.S.L., D.S. and O.T. All authors contributed to the final version of the manuscript.

Competing interests The authors declare no competing interests.

Additional information
Extended data is available for this paper at https://doi.org/10.1038/s41586-018-0592-2.
Supplementary information is available for this paper at https://doi.org/10.1038/s41586-018-0592-2.
Reprints and permissions information is available at http://www.nature.com/reprints.
Correspondence and requests for materials should be addressed to O.T.
Publisher's note: Springer Nature remains neutral with regard to jurisdictional claims in published maps and institutional affiliations.

© 2018 Springer Nature Limited. All rights reserved.

METHODS

Sample fabrication and the break junction technique. Our experiments were performed using a mechanically controllable break junction[25] setup located within a cryogenic chamber. The chamber is pumped to 10^{-5} mbar and then cooled down to the liquid helium temperature (4.2 K). This setup is placed in a specially designed Faraday cage to allow efficient noise measurements. The sample consists of a notched Au wire (99.99%, 0.1 mm diameter, 25 mm length, Goodfellow), which is attached to a flexible substrate (0.76 mm thick insulating Cirlex film). A three-point bending mechanism is used to bend the substrate in order to break the wire at the notch (Fig. 1a). The wire is first broken in cryogenic vacuum, to expose two clean atomically sharp tips that serve as the junction's electrodes. The breaking process is controlled by a piezoelectric element (PI P-882 PICMA), which is driven by a 24-bit NI-PCI4461 data acquisition (DAQ) card followed by a Piezomechanik SVR 150/1 piezo driver. These components provide fast and accurate control over the distance between the two tips with sub-ångström resolution. Conductance versus inter-electrode distance (conductance traces) were measured on bare Au junctions during repeated breaking and formation of the junction. Conductance histograms (for example, Extended Data Fig. 1) that provide the most probable conductance of the examined junction were constructed based on these traces to ensure that the junction exhibits the typical conductance characteristics of bare Au atomic-scale junctions[27,28].

To form molecular junctions, pure hydrogen gas (99.999%, Gas Technologies) was introduced to the junction via a stainless steel capillary that connects an external molecular source with the cryogenic environment. The flow of hydrogen was increased by increasing the hydrogen pressure up to about 10^{-2} mbar at the capillary input. The formation of Au/H_2 junctions was monitored during the insertion process by continuously recording conductance traces and producing a typical conductance histogram for Au/H_2 junctions (Extended Data Fig. 1). Following the formation of molecular junctions, the hydrogen flow was stopped. Further details concerning the characterization of molecular junctions are given in the Methods section 'Molecular junction characterization'.

Electronic measurement setup. To measure conductance traces, direct-current (d.c.) conductance is monitored while the junction is gradually broken by increasing the voltage applied on the piezoelectric element at a constant speed of 600 nm s^{-1} and a sampling rate of 100 kHz. The junction is biased with a constant voltage of 10–200 mV provided by a NI-PCI4461 DAQ card. The resulting current is amplified by a current preamplifier (SR570) and recorded by the DAQ card. Following each trace, the exposed atomic tips are pushed back into contact until the conductance reaches a value of at least $50G_0$, in order to ensure that the data consists of a statistical variety of different atomic scale junctions' geometries. Differential conductance measurements (dI/dV versus V) are conducted using a standard lock-in technique. A reference sine signal of 1 mV peak-to-peak voltage (Vpp) at about 3 kHz modulating a d.c. bias voltage is generated by the DAQ card. The alternating-current (a.c.) response is recorded by the DAQ card and extracted by a LabView implemented lock-in analysis to obtain the differential conductance as a function of bias voltage.

Extended Data Fig. 2 shows the electronic setup connected to the sample. The circuit can be switched between a conductance mode, which is used to measure the d.c. conductance of the examined junction and the dI/dV spectra, and a noise mode, applied to measure the noise generated by the junction. In the latter mode of measurement, the relatively noisy instruments used in the conductance mode are disconnected from the sample owing to the high sensitivity of the noise measurements. The voltage noise is amplified by a custom-made differential low-noise amplifier. The amplifier was calibrated by the thermal noise that is generated in a set of well-characterized resistors embedded in liquid nitrogen. A power spectrum between 0.25 kHz and 300 kHz is measured via a NI-PXI5922 DAQ card using a LabView implemented fast Fourier transform analysis and averaged 1,000 times. To assess the stability of our noise amplifier, we recorded the thermal noise temperature of junctions with different conductance values at the base temperature of the system in intervals of about 7 h. We did not observe any detectable shift in the obtained temperature. To measure shot noise, the sample is current-biased by a Yokogawa GS200 SC voltage source connected to the sample through two 1 MΩ resistors located in proximity to the sample. The total cabling length was minimized to reduce stray capacitance to about 40 pF. The low level of the measured noise signal from the sample makes it sensitive to extrinsic noise. To impede noise pickup, the measurement setup is located within a Faraday cage and all instruments are connected to a specially assigned quiet ground, and are optically isolated from a control computer outside the Faraday cage. All amplifiers are powered by batteries to avoid noise injection from power lines. Additionally, an RC filter (where R is resistance and C is capacitance) is connected after the piezo driver to minimize possible excitation of mechanical noise coupled to the junction through the piezoelectric element. The RC filter is bypassed when recording conductance traces in order to avoid interference with the measurements.

The temperature of each electrode is controlled by a feedback loop consisting a custom-made proportional–integral–derivative (PID) controller that is powered by batteries and located inside the Faraday cage, a heating resistor (thin-film, 100 Ω, Panasonic) that is thermally connected to each Au electrode by a sapphire housing, as well as a thermometer (Lakeshore DT-670 calibrated silicon diode) located at each electrode's tip (Fig. 1a). This feedback circuit is optically isolated from the control computer outside the Faraday cage. The system reaches an optimal stabilization around the preset temperature in about 35 min. Owing to the constant operation of a feedback loop, the actual temperature oscillates by at most 0.025 K around the set value. These variations are taken into consideration in the error calculations.

Molecular junction characterization. The typical conductance of gold atomic junctions is around $1G_0$, carried by one dominant transmission channel[28,29]. Since gold junctions with conductance below $0.7G_0$ frequently cannot be stabilized, we introduced hydrogen to form stable molecular junctions with a wider conductance range[23,24] below $1G_0$. This conductance window is necessary for the demonstration of the delta-T noise in Fig. 2. Before the introduction of molecules, the bare Au junction is characterized by constructing conductance histograms, as presented in Extended Data Fig. 1 (brown). The peak at $1G_0$, and the tail at low conductance are regarded as the typical fingerprints of a bare Au atomic junction[27,28]. The peak indicates the most probable conductance of a single atom Au junction (a single Au atom in the cross-section of the junction's constriction), while the tail at low conductance is the outcome of tunnelling conductance, measured after the breaking of a single atom junction. The blue conductance histogram exemplifies the different characteristics that emerge following the introduction of hydrogen. The large number of counts below $1G_0$ indicate the repeated formation of different stable molecular junction configurations with a broad range of conductance values. This feature of the studied molecular junctions allows us to perform noise measurements on stable junction configurations with a broad range of conductance below $1G_0$ (see Fig. 2 and Extended Data Fig. 8 for noise data obtained for hydrogen based molecular junctions and bare atomic gold junctions, respectively). In our setup, shot noise and delta-T noise give less reliable results below $0.1G_0$ owing to RC low-pass filtering. Therefore, we limit our analysis to junctions with conductance above $0.1G_0$.

Calibration of thermometers by thermal noise. Thermal noise identifies the electronic temperature that determines the Fermi–Dirac distribution of electrons in the electrodes (usually in a region of tens to hundreds of nanometres around the atomic scale junction). The silicon diode thermometers are attached to the surface of the electrodes near the electrode tips (Fig. 1a). The electric wires of these thermometers are anchored to metal thermalization plates at about 4.2 K to prevent the absorption of heat from their hot side, which is located outside the cryostat. As a result, when the sample is heated above the base temperature, the detected temperature by the thermometers is always lower than the thermal noise temperature. With the aid of thermal noise measurements, we could calibrate the temperature indicated by the thermometer to give the actual temperature in the nanoscale vicinity of the studied junction. The thermal noise was measured as a function of conductance at several fixed temperatures. The inset of Extended Data Fig. 3 provides an example for such a measurement at 37.10 ± 0.04 K (determined by a linear fit to the thermal noise). Then, the relation between the temperature given by the thermometers and the temperatures given by thermal noise was extracted for the relevant temperature range in our experiment (Extended Data Fig. 3). We note that the difference between the temperature measured by the thermometers and the temperature extracted from the thermal noise is nullified at the base temperature of the setup, as observed in Extended Data Fig. 3. This is due to the fact that at the base temperature, the thermalization plates that are connected to the wires of the thermometers have the same temperature as the junction, and they do not cool the thermometers to a lower temperature with respect to the junction's temperature. The calibration procedure described was used to relate a temperature at the nanoscale vicinity of the junction to the thermometer reads. This calibration reliably evaluates the electronic temperature at the electrode apexes, using macroscale thermometers. This procedure was performed before each experiment.

Shot noise measurements and shot noise analysis of Au/H_2 junctions. Shot noise measurements on Au/H_2 junctions were performed as described in refs [20,29]. Extended Data Fig. 4 presents the Fano factor, which is defined in the main text but is also equal to the measured shot noise in units of $2eI$ (where I is the current). The Fano factor is presented as a function of the corresponding conductance; both are obtained for different realizations of the Au/H_2 junctions. Junctions that are characterized by conductance above $1G_0$, which is the typical conductance of gold single-atom junctions, are obtained by squeezing the two electrodes against each other to form contacts with more than one Au atom at the narrowest cross-section of the contact, possibly contaminated by hydrogen.

The red curve in Extended Data Fig. 4 indicates the minimal Fano factor that is obtained by a sequential opening of channels, which can be described as follows. The first channel gradually opens between 0 and $1G_0$, with a transmission probability being equal to the conductance. The second channel opens above $1G_0$, with a transmission probability of $G/G_0 - 1$, since the first channel is kept fully open

© 2018 Springer Nature Limited. All rights reserved.

($\tau_1 = 1$), and so on. Therefore, molecular junctions with a Fano factor versus conductance that are located on the red curve below $1G_0$ are characterized by a single transmission channel. In fact, the bulk of the data below $1G_0$ accumulates close to this curve, indicating that the electronic transport of most molecular junctions is dictated by a single transmission channel with minor contributions from secondary channels (see inset I in Extended Data Fig. 4). Some of the data points at $1G_0$ show full suppression of the Fano factor. In these cases, the conductance is determined by a single channel with transmission probability of one. The dashed black line, which practically serves as the upper limit for the measured data below $1G_0$, indicates the maximal Fano factor that can be obtained for two channels (along the dashed line, the two channels have equal transmission probability). The Fano factor is insensitive to the conductance above $4G_0$ (ref. [29]), which is the relevant range for the thermal noise analysis presented in Fig. 1. In this conductance range, the Fano factor scatters around the averaged value of 0.28 with a standard deviation of 0.07.

Ratio between delta-T noise and thermal noise above $4G_0$. For $G > 4G_0$ we can assume a constant Fano factor ($F = 0.2$–0.4). The ratio between the delta-T noise ($S_{\Delta T}$) and the thermal noise (S_{TN}) is

$$\frac{S_{\Delta T}}{S_{TN}} = \frac{k_B G_0 F[(\Delta T)^2/\bar{T}](\pi^2/9 - 2/3)}{4k_B G_0 \bar{T}} = \frac{F}{4}\left(\frac{\Delta T}{\bar{T}}\right)^2\left(\frac{\pi^2}{9} - \frac{2}{3}\right) \quad (3)$$

where

$$\left.\frac{S_{\Delta T}}{S_{TN}}\right|_{F=0.2} = 0.0215\left(\frac{\Delta T}{\bar{T}}\right)^2$$
$$\left.\frac{S_{\Delta T}}{S_{TN}}\right|_{F=0.4} = 0.043\left(\frac{\Delta T}{\bar{T}}\right)^2 \quad (4)$$

Thus, a maximal ratio of 5% is obtained in our measurements for the extreme case of $\Delta T = 22.9$ K, $\bar{T} = 21.3$ K, and $F = 0.4$. However, typically this ratio is about 3%.

Measurements of noise at finite temperature difference. Following the formation of an atomic scale junction with a fixed inter-electrode distance at a given temperature difference, a current versus voltage curve (Extended Data Fig. 5a) was measured and the conductance was determined from the curve's slope ($G = I/V$) at its linear regime around zero voltage. The noise at a given temperature difference was measured by switching to the noise circuit (Extended Data Fig. 2), and measuring the total noise versus frequency (Extended Data Fig. 5b). To ensure the stability of the junction during this process, a second current versus voltage measurement was performed right after the noise measurement by switching back to the conductance circuit. The entire procedure of the two current versus voltage measurements and noise measurement takes about 30 s. Only when the difference between the conductance values found before and after the noise measurement was less than about 1% was the noise measurement considered valid. The voltage noise of the measurement setup was measured separately for a fully formed junction (a short circuit) at the same ΔT and was subtracted from the total noise spectra obtained in the experiment. The typical voltage noise of our setup varies between 8.1×10^{-19} and 9.0×10^{-19} V^2 Hz^{-1} (0.90–0.95 nV Hz$^{-1/2}$). Extended Data Fig. 5b presents the measured total noise for a set of junctions that are characterized by different conductance values, given by the different slopes of the curves presented in Extended Data Fig. 5a.

The suppression of the noise as a function of frequency observed in Extended Data Fig. 5b is the outcome of low-pass *RC* suppression due to the finite resistance (R) and capacitance (C) of our setup. Furthermore, this noise contains a small yet finite contribution from the amplifier input current noise (S_I^{in}) that is also subject to *RC* suppression. To account for these two effects, C and S_I^{in} were determined by optimally fitting an *RC* function (taking into account the current noise contribution) to thousands of noise versus frequency spectra measured at different conductance (for example, Extended Data Fig. 5c) and temperature (for example, Extended Data Fig. 5d) in the relevant range of our analysis ($0.1G_0$–$7.0G_0$ and 5.4–50.4 K). The noise spectra were fitted to the following *RC* transfer function S (in units of V^2 Hz^{-1}):

$$S = \frac{S_0}{1 + (2\pi f RC)^2} \quad (5)$$

where f is the frequency and S_0 is the zero frequency total noise. The amplifier input current noise was obtained (in units of V^2 Hz^{-1}) by

$$S_0 = 4k_B TR + [S_I^{in}(f)]^2 R^2 \quad (6)$$

The term $4k_B TR$ is the voltage thermal noise (note that $\Delta T = 0$ during this procedure). The typical capacitance of our measurement system is $C = 42.4 \pm 0.1$ pF and the amplifier input current noise (in units of A^2 Hz^{-1}) is $S_I^{in}(f) = 1.37 \times 10^{-32} \times f$, which has a linear dependence on frequency.

Once C and S_I^{in} are determined, every total noise spectrum that is measured at a finite temperature difference (Extended Data Fig. 5b) is corrected by the inverse of the *RC* function, using the obtained resistance from conductance measurements ($R = 1/G$; Extended Data Fig. 5a). S_I^{in} is then subtracted from the total noise to obtain the corrected total noise, presented in Extended Data Fig. 5e). Finally, every noise spectrum is averaged in a selected frequency window of 180–230 kHz, as seen in Extended Data Fig. 5e (the results are not sensitive to the selected range). The average values of the total noise as a function of conductance appear in Extended Data Fig. 5f, where the units are converted to A^2 Hz^{-1} by dividing each averaged value by the square of the corresponding resistance.

The contribution of shot noise generated by thermovoltage. To reveal the contribution of shot noise due to the generated thermovoltage in our measurement setup, the total thermovoltage of the system (sample and wires) was measured at the maximal temperature difference considered in Figs. 2 and 3. The measurement procedure is based on the technique described in ref. [30]. In Extended Data Fig. 6a we present the measured total thermovoltage as a function of conductance for the Au/H_2 junctions at $\Delta T = 25.3 \pm 0.6$ K and $\bar{T} = 26.3 \pm 0.7$ K. The scattering of the total thermovoltage for different junctions is more pronounced below $1G_0$, probably owing to the increased sensitivity of the transmission dependence on energy to structural variations when an atomic constriction is formed in the junction. A similar increase in the scattering of the data below $1G_0$ was observed in thermopower measurements on bare gold atomic junctions[31].

To estimate the maximal shot noise that can be generated in our experiments, we used equation (1) to calculate the shot noise that is expected for 155 μV, which is the largest thermovoltage acquired in our measurements (red star in Extended Data Fig. 6a). The obtained shot noise is plotted in red in Extended Data Fig. 6b along with the measured excess noise at the same average temperature and temperature difference. The largest expected shot noise due to the generation of thermovoltage in the junction is about three orders of magnitude smaller than the measured excess noise at a finite temperature difference. Thus, the observed excess noise in our experiments is not an outcome of the standard shot noise, and the fraction of shot noise contribution to this noise is practically negligible.

Fano factor based on delta-T noise measurements. Since the delta-T noise (second term in equation (2)) depends on $\sum_i \tau_i(1-\tau_i)$, the Fano factor $F = \sum_i \tau_i(1-\tau_i)/\sum_i \tau_i$ can be obtained from conductance ($G = G_0 \sum_i \tau_i$) and delta-T noise measurements, rather than by measuring the standard voltage-activated shot noise, which is the usual approach. Extended Data Fig. 9 presents the Fano factor versus conductance, obtained from noise measurements at a finite temperature difference and zero applied voltage. The overall behaviour is similar to the one presented in Extended Data Fig. 4. This agreement serves as an additional indication that the excess noise is in fact due to the delta-T noise. Furthermore, it illustrates that information about the distribution of transmission channels can be obtained from delta-T noise measurements.

Data availability

The datasets generated and analysed during this study are available from the corresponding author on reasonable request.

27. Ludoph, B., Devoret, M. H., Esteve, D., Urbina, C. & Van Ruitenbeek, J. M. Evidence for saturation of channel transmission from conductance fluctuations in atomic-size point contacts. *Phys. Rev. Lett.* **82**, 1530 (1999).
28. Rubio-Bollinger, G. et al. Single-channel transmission in gold one-atom contacts and chains. *Phys. Rev. B* **67**, 121407 (2003).
29. Vardimon, R., Matt, M., Nielaba, P., Cuevas, J. C. & Tal, O. Orbital origin of the electrical conduction in ferromagnetic atomic-size contacts: insights from shot noise measurements and theoretical simulations. *Phys. Rev. B* **93**, 085439 (2016).
30. Evangeli, C. et al. Engineering the thermopower of C_{60} molecular junctions. *Nano Lett.* **13**, 2141–2145 (2013).
31. Ludoph, B. & Van Ruitenbeek, J. M. Thermopower of atomic-size metallic contacts. *Phys. Rev. B* **59**, 12290 (1999).
32. Vardimon, R., Klionsky, M. & Tal, O. Experimental determination of conduction channels in atomic-scale conductors based on shot noise measurements. *Phys. Rev. B* **88**, 161404 (2013).

© 2018 Springer Nature Limited. All rights reserved.

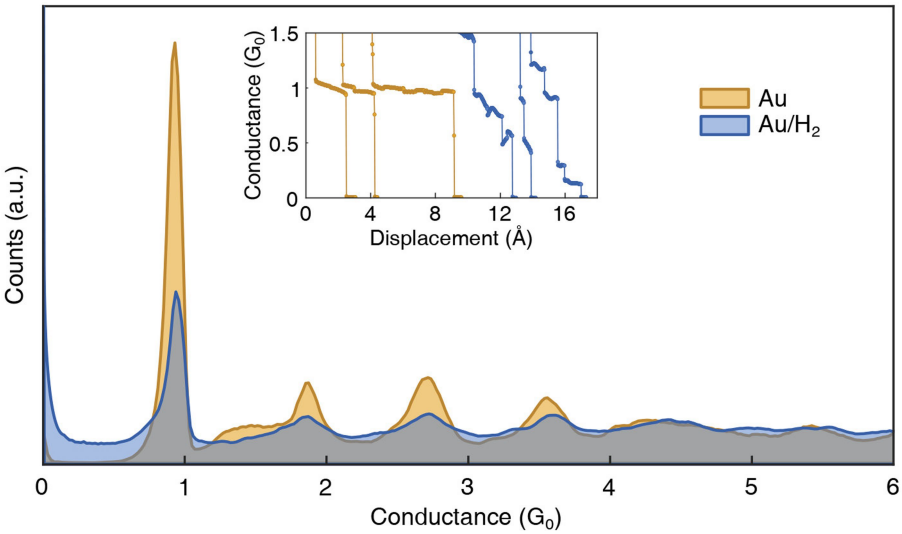

Extended Data Fig. 1 | Characterization of Au/H_2 molecular junctions. Conductance histograms of bare Au atomic junctions (brown) and Au/H_2 molecular junctions (blue) are shown. The histograms are composed from at least 1,500 conductance versus electrode displacement traces recorded at a bias voltage of 100 mV. a.u., arbitrary units.

© 2018 Springer Nature Limited. All rights reserved.

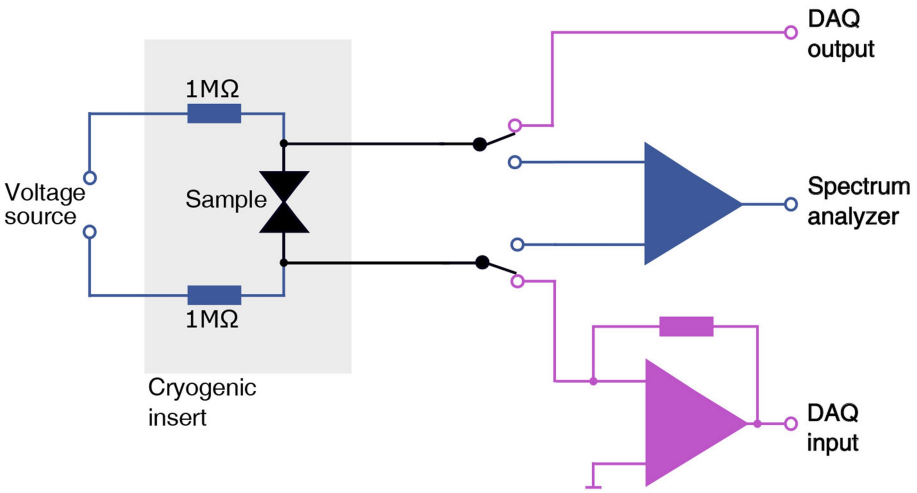

Extended Data Fig. 2 | Electronic measurement setup. Schematic presentation of the electronic circuit for conductance and noise measurements is shown. The electronic circuit consists of two switchable measurement circuits: a conductance circuit (purple) and a noise circuit (blue).

© 2018 Springer Nature Limited. All rights reserved.

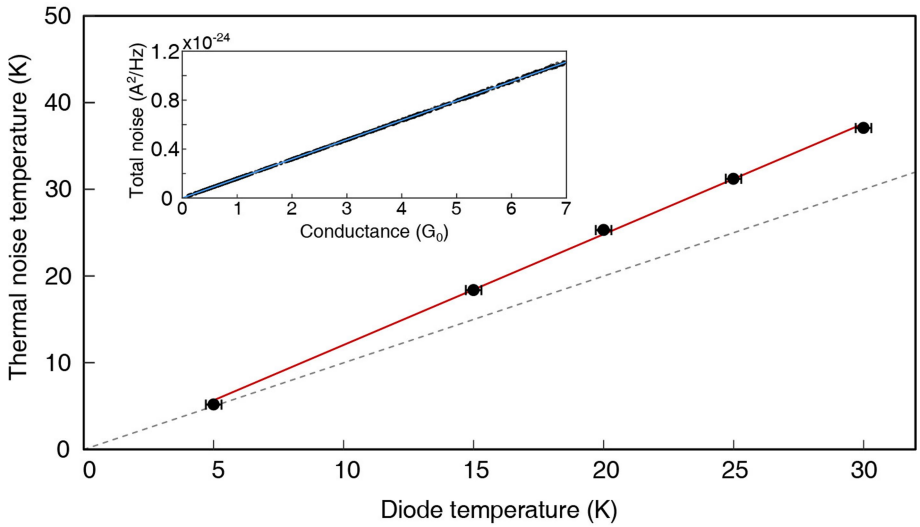

Extended Data Fig. 3 | Thermometer calibration based on thermal noise. The temperature measured by thermal noise is shown versus that measured using the diode thermometer (black circles; the vertical error bars are smaller than the circles' diameter). The error bars correspond to the systematic errors in our measurements. To guide the eye, the dashed grey line corresponds to a ratio of 1:1. The red line is a linear fit of the data. The calibration of the thermometers temperature is done by this fit $T_{TN} = (1.28 \pm 0.02) T_{therm} - 1.0 \pm 0.5$ K, where T_{therm} is the temperature measured by the thermometer. The inset shows an example for measured thermal noise versus conductance (black dots) at a thermal noise temperature of 37.10 ± 0.04 K. The blue line is a linear fit from which the thermal noise temperature is determined. This measurement procedure is repeated at different temperatures to construct the main graph. When the junction is heated above the setup base temperature, the thermometers attached to the electrode tips always indicate lower temperatures than those determined by the thermal noise.

© 2018 Springer Nature Limited. All rights reserved.

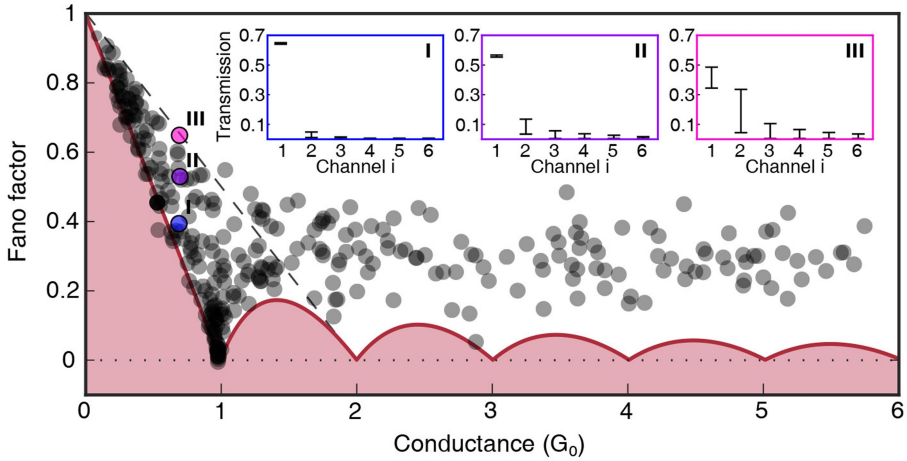

Extended Data Fig. 4 | Shot noise analysis for Au/H_2 junctions. The Fano factor extracted from shot noise and conductance measurements[20,29] is shown versus the conductance for different junction realizations at 4.6 K ($\Delta T = 0$). The thick red curve provides the minimal Fano factor. Data that accumulate on this line below $1G_0$ indicate junctions with a single transmission channel[22]. The dashed line provides the maximal Fano factor that two channels can generate for the relevant conductance. The insets show transmission probabilities of the main six transmission channels based on numerical analysis of the measured Fano factor and conductance[32] for the three marked cases (I, II, III) in the main panel. The error bars provide the range of transmission solutions that satisfies the measured conductance and shot noise. Inset I shows that a junction that is characterized by Fano factor and conductance data near the red curve conducts via a single dominant channel with only minor contribution from a secondary channel. In contrast, inset III exemplifies that a junction with Fano factor and conductance data near the dashed curve can conduct via two dominant channels with possible minor contributions from other channels.

© 2018 Springer Nature Limited. All rights reserved.

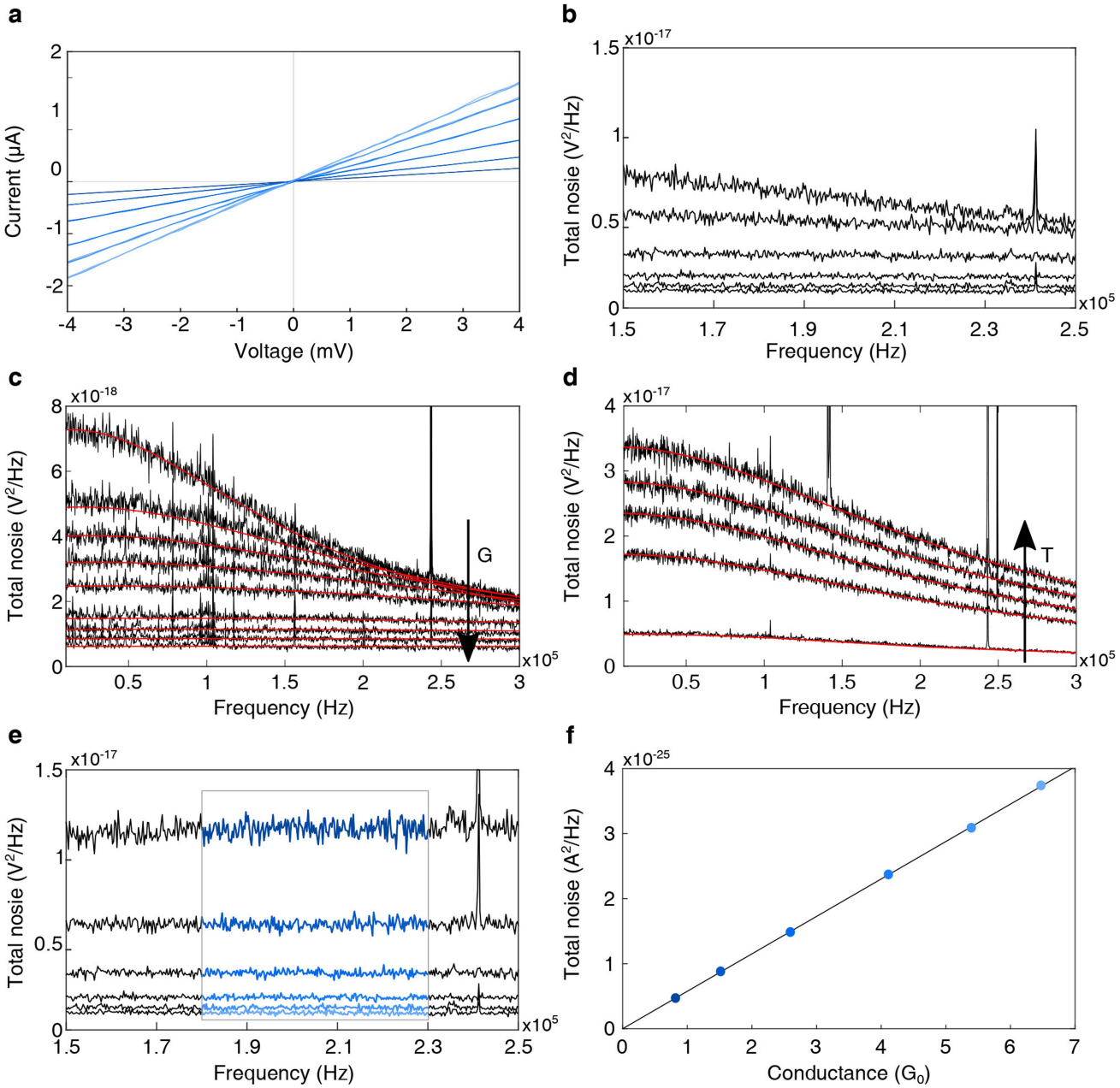

Extended Data Fig. 5 | Noise measurements at finite temperature differences. a, Current–voltage curves for a set of different junction realizations at $\bar{T} = 13.3 \pm 0.3$ K and $\Delta T = 12.6 \pm 0.2$ K. The conductance of each junction is obtained by the slope of the curve. Here, $G = 0.82G_0$, $1.52G_0$, $2.57G_0$, $4.05G_0$, $5.30G_0$ and $6.34G_0$, with all values $\pm 0.01G_0$, starting from the smallest slope. **b**, Total noise as a function of frequency for the same junctions examined in **a**. The top spectrum corresponds to the junction with the highest conductance. The noise is suppressed by low-pass *RC* filtering owing to the capacitance of the setup and the finite sample and wire resistance. **c**, Examples for *RC* transfer function and S_I^{in} fitting to spectra of total noise versus frequency measured at a fixed temperature of 5.4 ± 0.5 K, and different conductance values ($0.51G_0$–$6.03G_0 \pm 0.01G_0$). The arrow points in the direction of increasing conductance *G*. **d**, Same as **c** at a fixed conductance of $G = 0.77G_0 \pm 0.01G_0$, and different temperatures (5.4 ± 0.5 K to 37.5 ± 0.9 K). The arrow points in the direction of increasing temperature *T*. The setup capacitance and S_I^{in} are extracted from the fitting. **e**, The data presented in **b** corrected by an *RC* transfer function followed by subtraction of S_I^{in}. **f**, Total noise as a function of conductance obtained by averaging the noise presented in **e** in a frequency range of 180–230 kHz, coloured blue in **e**.

© 2018 Springer Nature Limited. All rights reserved.

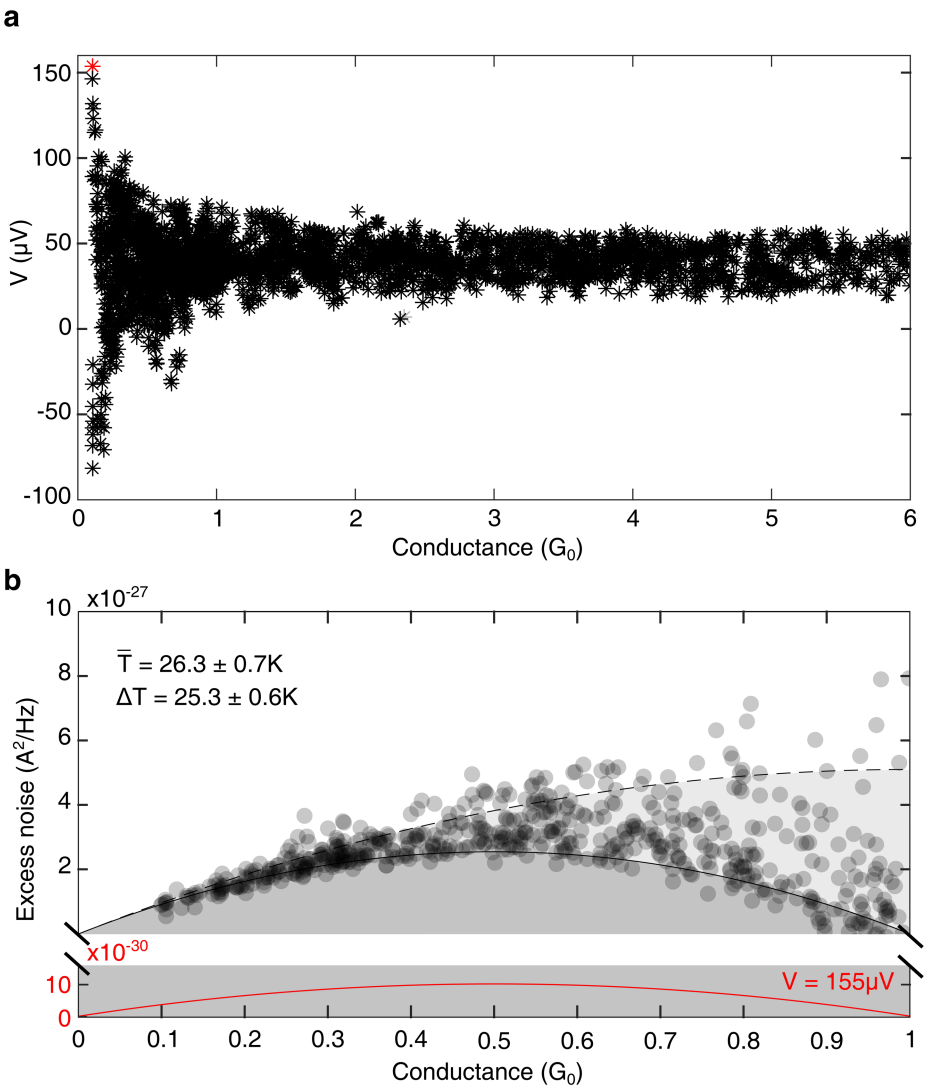

Extended Data Fig. 6 | Total thermoelectric voltage and its estimated contribution to the excess noise. a, Measured total thermoelectric voltage for the examined junctions as a function of conductance at $\bar{T} = 26.3 \pm 0.7$ K and $\Delta T = 25.3 \pm 0.6$ K. Measurements were performed according to the method described in ref. [30]. Here, we are interested in the total thermoelectric voltage that is built across the junction, since it can be a source for shot noise. **b**, Calculated shot noise (red curve) that is expected for the maximal measured thermovoltage in **a** (155 μV, marked as a red star in **a**), and the measured excess noise (dark circles) at the same $\bar{T}$ and ΔT for which the thermoelectric voltage was measured. Calculated delta-T noise is given by the black curve for a single transmission channel, and by the dashed curve for two channels with equal transmission probabilities (non-approximated numerical calculations based on equation (S2) in Supplementary Information).

© 2018 Springer Nature Limited. All rights reserved.

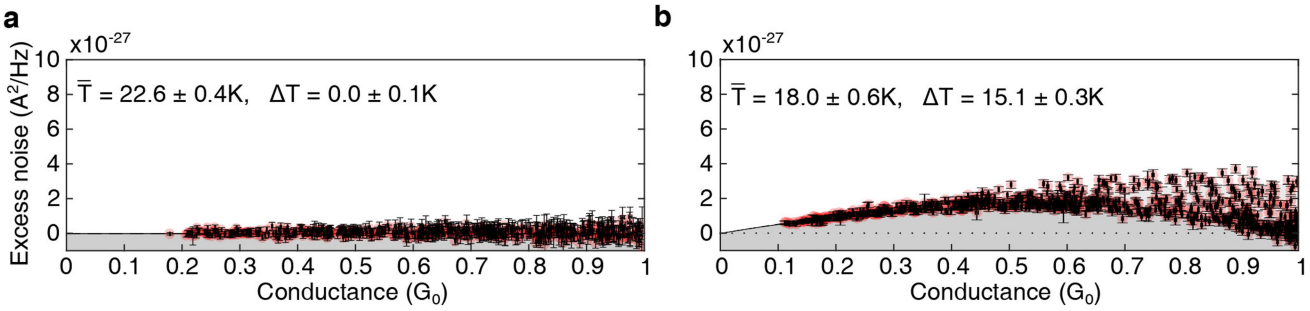

Extended Data Fig. 7 | Excess noise measured at zero and finite temperature difference with error bars. a, **b**, Excess noise as a function of conductance measured in the examined molecular junctions as presented in Fig. 2a, b, including error bars, corresponding to the systematic errors in our measurements. The size of the error bars is comparable or slightly larger than the diameter of the semitransparent red symbols.

© 2018 Springer Nature Limited. All rights reserved.

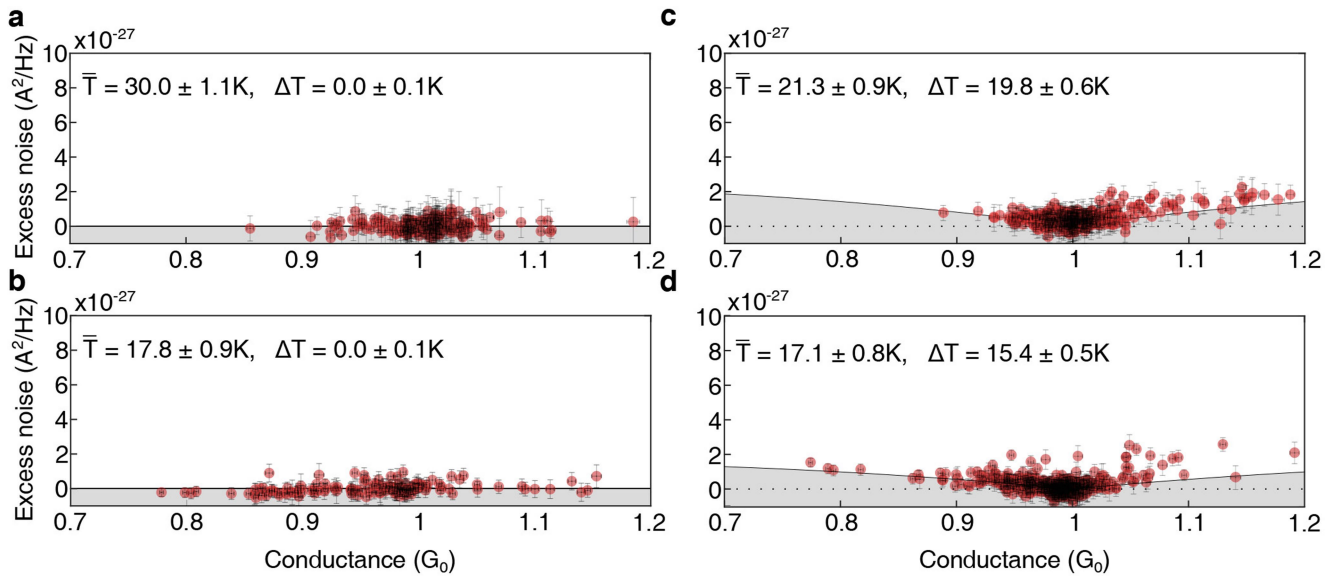

Extended Data Fig. 8 | Excess noise measured at zero and finite temperature difference for bare gold atomic junctions. a, **b**, Excess noise (obtained by subtracting the average thermal noise from the total measured noise) as a function of conductance measured in bare gold atomic junctions at different temperatures at thermal equilibrium ($\Delta T = 0$). **c**, **d**, Excess noise as a function of conductance measured at different average temperatures and finite temperature differences across the junctions ($\Delta T \neq 0$). Calculated delta-T noise is given by the black curve for single transmission channel probabilities (non-approximated numerical calculations based on equation (S2) in Supplementary Information). When a temperature difference is applied across the junctions, some enhancement of the excess noise is observed. The measured excess noise can be described by the theoretical expression for the delta-T noise, although the agreement is less clear than for hydrogen-based molecular junctions (Fig. 2), owing to the lack of data below $0.75G_0$. The spread in the results is a natural outcome of additional transmission channels that open as the conductance increases. The error bars correspond to the systematic errors in our measurements.

© 2018 Springer Nature Limited. All rights reserved.

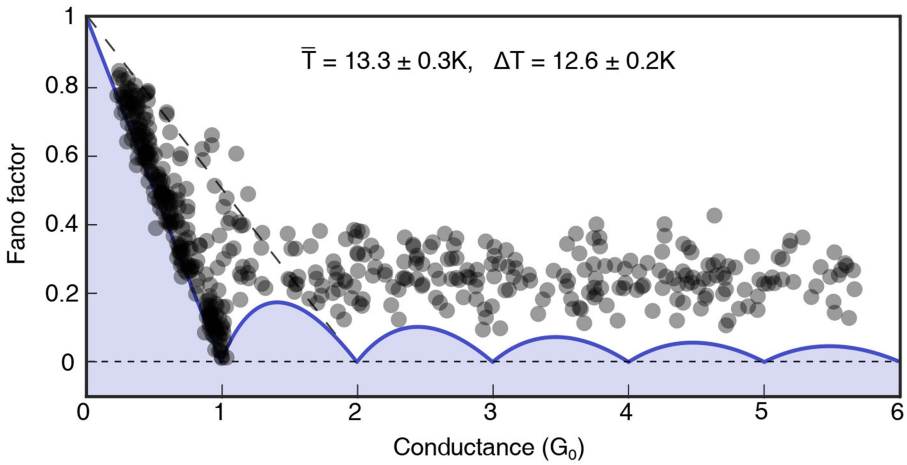

Extended Data Fig. 9 | Fano factor obtained from noise measurements at a finite temperature difference. The Fano factor (semitransparent black symbols) is extracted from the excess noise data presented in Fig. 2d, and the associated measured conductance using equation (2). The short-dashed horizontal line marks the zero Fano factor as a baseline. The thick blue curve provides the theoretically predicted minimal Fano factor. Data that accumulate on this line below $1G_0$ indicate junctions with a single transmission channel[22]. The long-dashed sloped line marks the maximal Fano factor that two channels can generate for the relevant conductance.

© 2018 Springer Nature Limited. All rights reserved.

nature

SUPPLEMENTARY INFORMATION

https://doi.org/10.1038/s41586-018-0592-2

In the format provided by the authors and unedited.

Electronic noise due to temperature differences in atomic-scale junctions

Ofir Shein Lumbroso[1], Lena Simine[2,3], Abraham Nitzan[4,5], Dvira Segal[2] & Oren Tal[1]*

[1]Department of Chemical and Biological Physics, Weizmann Institute of Science, Rehovot, Israel. [2]Department of Chemistry, University of Toronto, Toronto, Ontario, Canada. [3]Department of Chemistry, Rice University, Houston, TX, USA. [4]Department of Chemistry, University of Pennsylvania, Philadelphia, PA, USA. [5]School of Chemistry, Tel Aviv University, Tel Aviv, Israel. *e-mail: oren.tal@weizmann.ac.il

© 2018 Springer Nature Limited. All rights reserved.

Supplementary Information

Electronic noise due to temperature differences in atomic-scale junctions

Authors: Ofir Shein Lumbroso[1], Lena Simine[2,3], Abraham Nitzan[4,5], Dvira Segal[2], and Oren Tal[1]

Affiliations: [1]Department of Chemical and Biological Physics, Weizmann Institute of Science, Rehovot, Israel

[2]Department of Chemistry, University of Toronto, Toronto, Ontario, Canada

[3]Department of Chemistry, Rice University, Houston, Texas, USA

[4]Department of Chemistry, University of Pennsylvania, Philadelphia, Pennsylvania, USA

[5]School of Chemistry, Tel Aviv University, Tel Aviv, Israel

Analytical Results:

The full counting statistics of charge transport in multi-terminal conductors can be obtained analytically for noninteracting carriers[33,34]. In this supplementary material, we consider two-terminal junctions under both voltage and temperature biases. Assuming spin-degeneracy, the charge current through a single channel is given by the Landauer formula

$$I = \frac{2e}{h}\int_{-\infty}^{\infty} d\epsilon \tau(\epsilon)[f_L(\epsilon,\mu_L,T_L) - f_R(\epsilon,\mu_R,T_R)]. \quad \text{(S1)}$$

Here, $f_v(\epsilon,\mu_v,T_v) = \left[e^{\beta_v(\epsilon-\mu_v)}+1\right]^{-1}$, is the Fermi-Dirac distribution function, $v = L,R$, with the inverse temperature $\beta = 1/(k_B T)$ and chemical potential μ. Henceforth, unless otherwise stated, integrals are performed in the full range [-∞, ∞]. However, in fact the thermal energy and the voltage bias determine the relevant domain of integration. In particular, at zero bias all integrals contribute only in the vicinity of the Fermi energy, within the thermal broadening, as we show below. Thus, the upper and lower integration limits do not influence the results.

At the same level of description as Eq. (S1), the spectral density of the current noise can be written as $S_I = S_1 + S_2$[8], with the two components

$$S_1 = \frac{4e^2}{h}\int d\epsilon\{f_L(\epsilon,\mu_L,T_L)[1-f_L(\epsilon,\mu_L,T_L)] + f_R(\epsilon,\mu_R,T_R)[1-f_R(\epsilon,\mu_R,T_R)]\}[\tau(\epsilon)]^2,$$
$$S_2 = \frac{4e^2}{h}\int d\epsilon\{f_R(\epsilon,\mu_R,T_R)[1-f_L(\epsilon,\mu_L,T_L)] + f_L(\epsilon,\mu_L,T_L)[1-f_R(\epsilon,\mu_R,T_R)]\}\tau(\epsilon)[1-\tau(\epsilon)]. \quad \text{(S2)}$$

The single-channel transmission function $\tau(\epsilon)$ generally varies with energy. In what follows, we take it as a constant, τ. Based on this approximation, we evaluate S_1 exactly by using identities for the Fermi function,

$$S_1 = \frac{4e^2}{h}\tau^2\int d\epsilon\left[-k_BT_L\frac{\partial f_L}{\partial\epsilon} - k_BT_R\frac{\partial f_R}{\partial\epsilon}\right] = \frac{4e^2}{h}\tau^2 k_B(T_L+T_R). \quad \text{(S3)}$$

To evaluate S_2, we Taylor-expand it around equilibrium with $\Delta\mu = \mu_L - \mu_R = eV$ and $\Delta T = T_L - T_R$,

$$S_2 \approx S_2(\Delta\mu,\Delta T=0) + S_2(\Delta\mu=0,\Delta T) - S_2(\Delta\mu=0,\Delta T=0) + S_2(\Delta\mu\neq 0,\Delta T\neq 0)\,. \quad \text{(S4)}$$

The first term accounts for finite-voltage effects at fixed temperature. The second term similarly includes all contributions that depend on the temperature difference, at zero voltage bias. We subtract the equilibrium value to eliminate double counting. The last, fourth element collects mixed voltage-bias and temperature-bias terms. The equilibrium contribution can be readily obtained, with

$$S_2(\Delta\mu=0,\Delta T=0) = \frac{4e^2}{h}\,\tau(1-\tau)2k_B\bar{T}. \quad \text{(S5)}$$

Here, $\bar{T} = (T_L+T_R)/2$. The separate voltage and temperature-induced terms can be organized as follows,

$$S_2(\Delta\mu,\Delta T=0) = \frac{4e^2}{h}\,\tau(1-\tau)\int d\epsilon\,[f_L(\epsilon,\mu_L,\bar{T}) - f_R(\epsilon,\mu_R,\bar{T})]\coth\left(\frac{\Delta\mu}{2k_B\bar{T}}\right)$$
$$= \frac{4e^2}{h}\,\tau(1-\tau)\,\Delta\mu\coth\left(\frac{\Delta\mu}{2k_B\bar{T}}\right), \quad \text{(S6)}$$

and

$$S_2(\Delta\mu=0,\Delta T) = \frac{4e^2}{h}\,\tau(1-\tau)\int d\epsilon\,[f_L(\epsilon,\mu,T_L) - f_R(\epsilon,\mu,T_R)]\coth\left(\frac{(T_L-T_R)}{2k_BT_LT_R}(\epsilon-\mu)\right). \quad \text{(S7)}$$

We simplify (S7) by Taylor expanding the two functions setting $\mu = 0$ and $\Delta\beta = \beta_R - \beta_L > 0$,

$$\coth(\Delta\beta\epsilon/2) \approx \frac{2}{\Delta\beta\epsilon} + \frac{\Delta\beta\epsilon}{6} - \frac{(\Delta\beta)^3\epsilon^3}{360} + O(\Delta\beta^5)$$

$$f_L(\epsilon,\mu,T_L) - f_R(\epsilon,\mu,T_R) \approx \Delta T\frac{\partial f}{\partial \bar{T}} + \frac{1}{24}(\Delta T)^3\frac{\partial^3 f}{\partial \bar{T}^3} + \frac{1}{16\times 5!}(\Delta T)^5\frac{\partial^5 f}{\partial \bar{T}^5} + \ldots$$

Here, $f(\epsilon,\mu,\bar{T}) = \left[e^{(\epsilon-\mu)/\bar{T}} + 1\right]^{-1}$ is the equilibrium Fermi function. We substitute these expansions into Eq. (S7), integrate, and collect terms up to $(\Delta T)^2$,

$$S_2(\Delta\mu = 0, \Delta T) = \frac{4e^2}{h}\tau(1-\tau)k_B\left[(T_L + T_R) + \frac{(T_L - T_R)^2}{2\bar{T}}\left(\frac{\pi^2}{9} - \frac{2}{3}\right)\right]. \tag{S8}$$

Note that odd powers in ΔT do not contribute since the junction conducts symmetrically in the forward and backward directions. We also perform a direct expansion of Eq. (S2) to identify mixed temperature bias - voltage bias contributions. Collecting all terms into Eq. (S4), we obtain an approximate expression for the total noise, $S_I = S_1 + S_2$, with

$$S_1 = \frac{4e^2}{h}\tau^2 k_B(T_L + T_R)$$

$$S_2 \approx \frac{4e^2}{h}\tau(1-\tau)\left[\Delta\mu\coth\left(\frac{\Delta\mu}{2k_B\bar{T}}\right) - 2k_B\bar{T}\right]$$

$$+\frac{4e^2}{h}\tau(1-\tau)k_B\left[(T_L + T_R) + \frac{(T_L - T_R)^2}{2\bar{T}}\left(\frac{\pi^2}{9} - \frac{2}{3}\right)\right]$$

$$+\frac{4e^2}{h}\left.\frac{\partial\tau}{\partial\epsilon}\right|_\mu (1-2\tau)(T_L - T_R)\Delta\mu\frac{k_B}{2}\left(\frac{\pi^2}{9} - \frac{2}{3}\right). \tag{S9}$$

This expression generalizes the Johnson-Nyquist thermal noise and the voltage-biased shot noise limit, and it reduces to the correct expressions in the appropriate limits. Note that mixed temperature bias – voltage bias terms depend on the derivative of the transmission function at the vicinity of the Fermi energy. In our junctions, this variation is negligible, as can be deduced from the minor thermoelectric response (Extended Data Fig. 6)[15].

We now highlight the case presented in the main text, when a temperature difference is applied, with $\Delta T = T_h - T_c$ and $\bar{T} = (T_h + T_c)/2$, missing bias voltage, and insignificant $\left.\frac{\partial \tau}{\partial \epsilon}\right|_{\mu}$. The total noise from (S9) is given by ($G_0 \equiv 2e^2/h$),

$$S_I \approx 4k_B \bar{T} G_0 \tau + \left[\frac{k_B(\Delta T)^2}{\bar{T}}\left(\frac{\pi^2}{9} - \frac{2}{3}\right)\right] G_0\, \tau(1-\tau)\,. \qquad \text{(S10)}$$

For the multi-channels case (equation (2) in the main text), τ is replaced by $\sum_i \tau_i$, and $\tau(1-\tau)$ by $\sum_i \tau_i\,(1-\tau_i)$. It is important to understand the range of validity of this expression. We received it by Taylor expanding Eq. (S7) up to terms proportional to ΔT^2. However, as we argue next, Eq. (S10) serves in fact as an excellent approximation for the delta-T noise even furthest beyond linear response, at the extreme point when $\Delta T = 2\bar{T}$. In Figure S1, we analyze the contribution of the different functions in Eq. (S7). In panel (a) we display the $\coth\left(\frac{\epsilon\Delta\beta}{2}\right)$ function as a function of $\epsilon\Delta\beta$ with $\Delta\beta = \beta^c - \beta^h$; the chemical potential μ is taken as a reference point. The function is odd. It takes high values for $|\epsilon\Delta\beta| < 1$, beyond which it reaches an asymptotic value of ± 1. Given a characteristic experiment with $T_h = 40$ K, $T_c = 20$ K, we note that $\Delta\beta \cong 300$ in units of $(eV)^{-1}$. Therefore, the main contribution to the

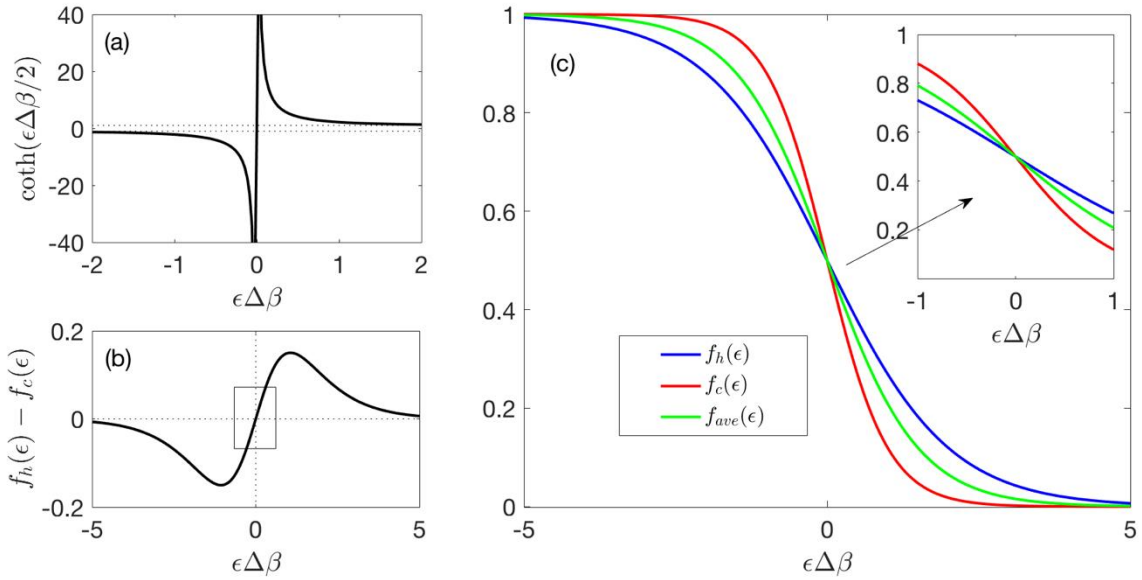

Figure S1. Analysis of the different functions in Eq. (S7). We use $T_h = 40$ K, $T_c = 20$ K, which results in $\Delta\beta \cong 300$ in units of $(eV)^{-1}$.

integral arises from low energy contributions, $\frac{1}{\Delta\beta}$ ~ 3 meV. In panel (b) we show the difference of the Fermi functions of the cold and hot metal leads. In panel (c) we further display the Fermi functions themselves, as well as the Fermi function evaluated at $\bar{T}$. In the relevant range of $|\epsilon\Delta\beta| < 1$, the hot and cold distribution functions only mildly deviate from the equilibrium function, justifying a second order expansion. This is particularly clear when inspecting panel (b): The box highlights the region that mostly contributes to the integral, given the structure of the $\coth\left(\frac{\epsilon\Delta\beta}{2}\right)$ function in panel (a). It is also useful to note that the noise S_I includes only even powers in ΔT. Therefore, the next term in the series is of order ΔT^4. We calculate this quartic contribution and find that it is proportional to $C_4\frac{\Delta T^4}{\bar{T}^3}$, with $C_4 = 2\left[\frac{\pi^2}{72} - \frac{1}{24} + \frac{1}{40} - \frac{7}{15}\frac{\pi^4}{360}\right]$. Recall that the quadratic term in Eq. (S10) is proportional to $C_2\frac{\Delta T^2}{\bar{T}}$ with $C_2 = \left(\frac{\pi^2}{9} - \frac{2}{3}\right)$. We compare the quartic to the quadratic contribution and reveal that even beyond linear response, when $\Delta T = 2\bar{T}$, the quartic contribution is inconsequential relative to the quadratic term.

In Figure S2, we compare the excess noise as obtained from the direct numerical evaluation of the integrals in Eq. (S2), $S_I(\bar{T}, \Delta T) - S_I(\bar{T}, \Delta T = 0)$, to the quadratic (second) term in Eq. (S10). We consider temperatures corresponding to the experiment, Figure 2 in the main text. We confirm that the quadratic expression is remarkably accurate with up to 3% deviation from the numerical result. Furthermore, we show that the fourth order correction appears on top of the numerical result, see inset.

Partition noise can be generated by different sources such as a voltage bias, as is commonly done, or a temperature difference, as exemplified in this work. It is important to comment that these stimuli show marked differences. When a temperature difference is applied, in the absence of a voltage bias, the charge current is zero under the constant-transmission approximation. This can be proved by inspecting Eq. (S1); for simplicity, we set $\mu = 0$,

$$I(\Delta T) = \frac{2e}{h}\tau\int_{-\infty}^{\infty} d\epsilon\left[\frac{1}{e^{\beta_L\epsilon}+1} - \frac{1}{e^{\beta_R\epsilon}+1}\right] = \frac{2e}{h}\tau\int_{-\infty}^{\infty} d\epsilon\left[\frac{e^{\beta_R\epsilon} - e^{\beta_L\epsilon}}{(e^{\beta_L\epsilon}+1)(e^{\beta_R\epsilon}+1)}\right]. \quad \text{(S11)}$$

Since the integrand $F(\epsilon) \equiv \frac{e^{\beta_R\epsilon} - e^{\beta_L\epsilon}}{(e^{\beta_L\epsilon}+1)(e^{\beta_R\epsilon}+1)}$ is an odd function, $F(\epsilon) = -F(-\epsilon)$, the charge current is zero, $I(\Delta T) = 0$.

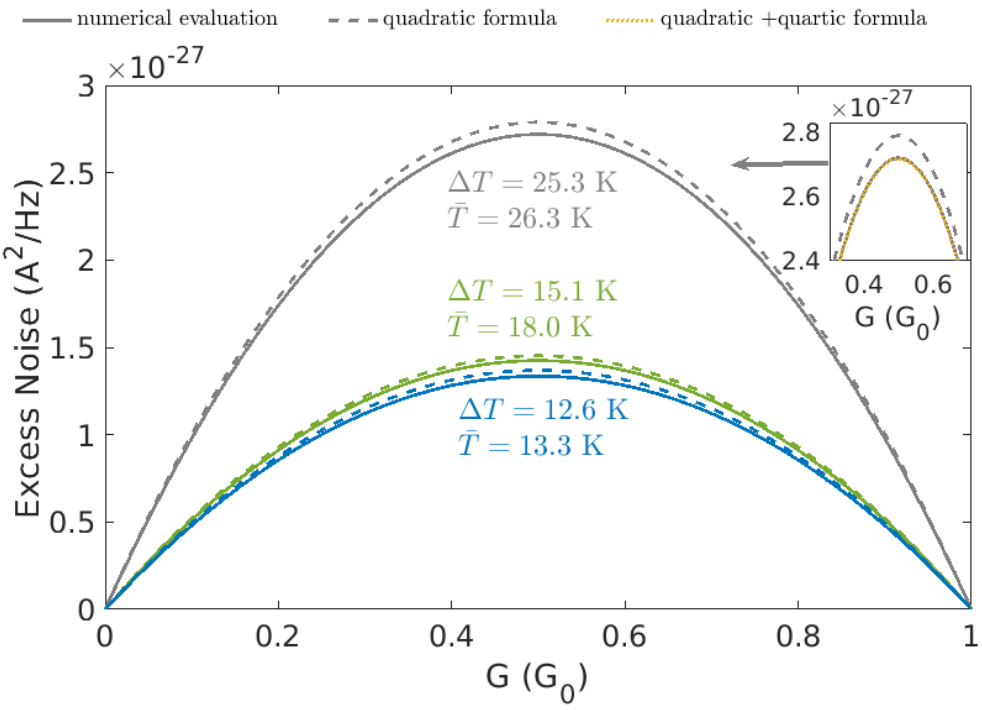

Figure S2. Excess noise: Numerical results vs. approximate quadratic formula. We compare the numerical solution of Eq. (S2), depicted in full line, to the approximated quadratic expression in Eq. (S10), dashed line. In the inset, corresponding to the highest averaged temperature, we further include the quartic correction (dotted), where the quadratic + quartic formula perfectly reproduces the numerical solution.

The first non-trivial contribution to the current is therefore related to the structure of the transmission function around the Fermi energy, in other words, to the thermopower S_{tp},

$$I(\Delta T) = \frac{2e}{h} \times \frac{\partial \tau}{\partial \epsilon}\Big|_{\mu} \int_{-\infty}^{\infty} \epsilon d\epsilon \left[\frac{1}{e^{\beta_L \epsilon}+1} - \frac{1}{e^{\beta_R \epsilon}+1}\right] = \frac{2e}{h} \times \frac{\partial \tau}{\partial \epsilon}\Big|_{\mu} \frac{\pi^2 k_B^2 \bar{T}}{3} \Delta T = G_0 \tau S_{tp} \Delta T. \quad \text{(S12)}$$

It is also useful to look at the energy current, which is nonzero under a temperature difference,

$$I_E(\Delta T) = \frac{2}{h} \tau \int_{-\infty}^{\infty} \epsilon d\epsilon \left[\frac{1}{e^{\beta_L \epsilon}+1} - \frac{1}{e^{\beta_R \epsilon}+1}\right] = \frac{1}{h} \tau \frac{2\pi^2 k_B^2 \bar{T}}{3} \Delta T. \quad \text{(S13)}$$

Note that the prefactor corresponds to the quantum of thermal conductance κ_Q, thus we arrive at the expected expression $I_E(\Delta T) = \kappa_Q \tau \Delta T$. In contrast, under applied voltage but in the absence of a temperature bias, the charge current is finite

$$I(V) = \frac{2e}{h}\tau \int_{-\infty}^{\infty} d\epsilon \left[\frac{1}{e^{\beta\left(\epsilon - \frac{eV}{2}\right)}+1} - \frac{1}{e^{\beta\left(\epsilon + \frac{eV}{2}\right)}+1} \right] = \frac{2e^2}{h}\tau V, \quad \text{(S14)}$$

but the energy current vanishes, $I_E(V) = 0$.

To conclude, Eq. (S10) serves as an excellent approximation to the thermal and delta-T noises. It holds even far from equilibrium - as long as the transmission function can be assumed constant for all incoming electrons in the thermal window. It is also interesting to note that if we replace the Fermi Dirac functions by their low-temperature approximation, $f(\epsilon, T) = \frac{1}{e^{\beta(\epsilon-\mu)}+1} \to e^{-\beta(\epsilon-\mu)}$, we can readily calculate the non-equilibrium noise $S_2(\Delta\mu = 0, \Delta T) = G_0\tau(1-\tau)k_B\left(4\bar{T} + \frac{\Delta T^2}{\bar{T}}\right)$. As a result, we receive Eq. (S10), only missing the numerical prefactor in front of the quadratic term. Note that this a qualitative argument: Since the main contribution to the integral arises from low-energy electrons, we have to properly describe the shape of the function for $|\beta\epsilon| \ll 1$.

References:

33. Levitov, L. S., Lee, H. & Lesovik G.B. Electron counting statistics and coherent states of electric current. *J. Math. Phys.* **37**, 4845 (1996).

34. Lee, H., Levitov, L. S. & Yakovets, A. Y. Universal statistics of transport in disordered conductors. *Phys. Rev. B* **51**, 4079 (1995).